AD-A161 062 CORRELATION OF RESULTS OF AN OH-58A HELICOPTER COMPOSITE TAIL BOOM TEST W..(U) ARMY AVIATION SYSTEMS COMMAND ST LOUIS MO N CALAPODAS ET AL. SEP 85 1/1

UNCLASSIFIED USAAVSCOM-TR-85-D-15 F/G 1/3 NL

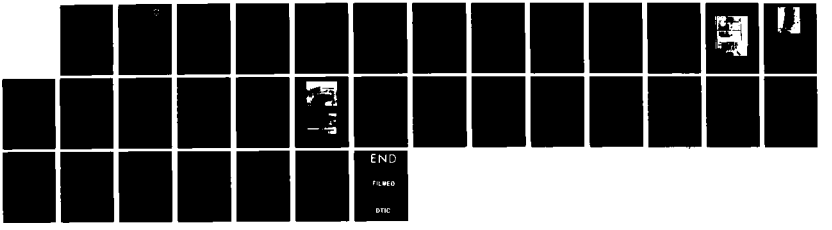

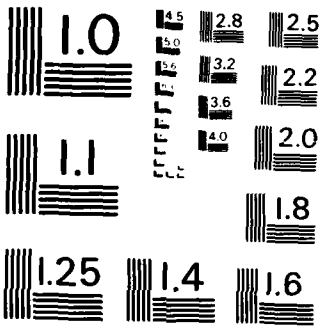

USAAVSCOM TR-85-D-15

CORRELATION OF RESULTS OF AN OH-58A HELICOPTER COMPOSITE TAIL BOOM TEST WITH A FINITE ELEMENT MODEL

Nick Calapodas
Keith Hoff

September 1985

AVIATION APPLIED TECHNOLOGY DIRECTORATE
US ARMY AVIATION RESEARCH AND TECHNOLOGY ACTIVITY (AVSCOM)
Fort Eustis, VA. 23604-5577

AVSCOM — PROVIDING LEADERS THE DECISIVE EDGE

DISCLAIMERS

The findings in this report are not to be construed as an official Department of the Army position unless so designated by other authorized documents.

When Government drawings, specifications, or other data are used for any purpose other than in connection with a definitely related Government procurement operation, the United States Government thereby incurs no responsibility nor any obligation whatsoever; and the fact that the Government may have formulated, furnished, or in any way supplied the said drawings, specifications, or other data is not to be regarded by implication or otherwise as in any manner licensing the holder or any other person or corporation, or conveying any rights or permission, to manufacture, use, or sell any patented invention that may in any way be related thereto.

Trade names cited in this report do not constitute an official endorsement or approval of the use of such commercial hardware or software.

DISPOSITION INSTRUCTIONS

Destroy this report by any method which precludes reconstruction of the document. Do not return it to the originator.

Unclassified
SECURITY CLASSIFICATION OF THIS PAGE

AD-A161 062

REPORT DOCUMENTATION PAGE

1a REPORT SECURITY CLASSIFICATION Unclassified	1b. RESTRICTIVE MARKINGS
2a. SECURITY CLASSIFICATION AUTHORITY	3 DISTRIBUTION / AVAILABILITY OF REPORT Approved for public release; distribution is unlimited.
2b. DECLASSIFICATION / DOWNGRADING SCHEDULE	
4 PERFORMING ORGANIZATION REPORT NUMBER(S) USAAVSCOM TR 85-D-15	5. MONITORING ORGANIZATION REPORT NUMBER(S)
6a NAME OF PERFORMING ORGANIZATION Aviation Applied Technology Directorate 6b OFFICE SYMBOL (If applicable)	7a. NAME OF MONITORING ORGANIZATION
6c ADDRESS (City, State, and ZIP Code) US Army Aviation Research and Technology Activity (AVSCOM) Fort Eustis, Virginia 23604-5577	7b. ADDRESS (City, State, and ZIP Code)
8a. NAME OF FUNDING / SPONSORING ORGANIZATION 8b. OFFICE SYMBOL (If applicable)	9 PROCUREMENT INSTRUMENT IDENTIFICATION NUMBER House Task 80-4
8c. ADDRESS (City, State, and ZIP Code)	10. SOURCE OF FUNDING NUMBERS PROGRAM ELEMENT NO. / PROJECT NO. 1L162209AH76 / TASK NO. / WORK UNIT ACCESSION NO.

11 TITLE (Include Security Classification)
Correlation of Results of an OH-58A Helicopter Composite Tail Boom Test With a Finite Element Model

12 PERSONAL AUTHOR(S)
Nick Calapodas and Keith Hoff

13a TYPE OF REPORT	13b TIME COVERED	14 DATE OF REPORT (Year, Month, Day)	15 PAGE COUNT
Technical Report	FROM _____ TO _____	September 1985	26

16 SUPPLEMENTARY NOTATION

17 COSATI CODES			18. SUBJECT TERMS (Continue on reverse if necessary and identify by block number)
FIELD	GROUP	SUB-GROUP	Helicopter, Composite, Primary Structure, Finite Element, Modeling, Correlation

19 ABSTRACT (Continue on reverse if necessary and identify by block number)

The purpose of this research effort was to evaluate modeling and testing complexities of composite structures. Static and dynamic tests of an OH-58A composite tail boom were conducted by personnel from the Aviation Applied Technology Directorate, US Army Aviation Research and Technology Activity (ARTA). The finite element model was developed and analyzed by personnel from the Aerostructures Directorate, ARTA; details of that effort are presented in a separate report.

The results of testing an OH-58A composite tail boom and comparing its static and dynamic characteristics with those obtained from finite element analyses are presented in this report. Static load versus deflection data were used to verify the stiffness representation of the finite element model. Ground vibration test data were used to evaluate frequency and modal responses obtained from analysis. Discussions of each test configuration, including data analysis methodology and correlation results, are presented. Differences between measured static deflections and finite element analysis calculated deflections ranged from 6 to 12 percent. Natural frequency differences between test and analysis were less than 5 percent for the first and second elastic modes. Problems encountered during the testing and the impact on correlation are also discussed.

20 DISTRIBUTION / AVAILABILITY OF ABSTRACT	21. ABSTRACT SECURITY CLASSIFICATION
☒ UNCLASSIFIED/UNLIMITED ☐ SAME AS RPT ☐ DTIC USERS	Unclassified
22a NAME OF RESPONSIBLE INDIVIDUAL Nick Calapodas	22b. TELEPHONE (Include Area Code) (804) 878-3822 / 22c. OFFICE SYMBOL SAVRT-TY-ATS

DD FORM 1473, 84 MAR — 83 APR edition may be used until exhausted. All other editions are obsolete.

SECURITY CLASSIFICATION OF THIS PAGE

TABLE OF CONTENTS

A1

LIST OF FIGURES

LIST OF TABLES

INTRODUCTION

The use of composite materials in helicopter structures adds a complex dimension relative to analytical predictions of helicopter static and dynamic characteristics. Fiber orientation, fiber/epoxy elastic properties, combinations of various fiber materials, and the overall structural configuration of composites require the use of more sophisticated modeling approaches. For a composite structure, the traditional skin/stringer configuration is replaced by continuous skin structures of solid laminate or sandwich honeycomb which become the primary load carriers. In the corresponding finite element (FE) representation, classical rod/bar and membrane elements that simulate the skin/stringer configuration are replaced by single quadrilateral plate elements capable of reacting both in-plane and bending loads.

The increased emphasis on the use of composite materials for helicopter applications by the US Army led to this program for examining the modeling and testing complexities of composite structures. An OH-58A composite tail boom was selected as the test specimen because of its availability and inherent complexities. Filament winding, integrally wound and secondarily bonded circumferential stiffening frames, tapered geometry, cutouts, nonuniform fiber orientation/lamination, and variations of fiber materials are examples of these complexities. This report presents a comparison of finite element analysis load/deflection and natural frequency predictions with data obtained from static and dynamic tests. The finite element modeling effort was performed at the Aerostructures Directorate, US Army Aviation Research and Technology Activity (ARTA), and the static and dynamic testing and data correlation were performed at the Aviation Applied Technology Directorate, ARTA.

TEST SPECIMEN DESCRIPTION

Descriptions of the OH-58A helicopter composite tail boom and the finite element model developed to predict tail boom static and dynamic characteristics are presented.

COMPOSITE TAIL BOOM STRUCTURE

The test specimen, an OH-58A composite tail boom, was obtained from the *Environmental Effects and Durability Evaluation of Advanced Composite Fuselage Structures* program (Reference 1). The test specimen (Figure 1), a toolproof article, differs slightly from flightworthy tail booms that were fabricated during the same program. The flightworthy tail booms have E-glass partial bulkheads bonded to the tail boom where the tail rotor drive shaft bearing supports are anchored and the tail rotor push-pull tube is inserted; these bulkheads were not on the test specimen. The tail boom has a circular cross section and a 2.31 taper ratio. Four integrally wound foam stabilized graphite frames and a graphite epoxy laminate skin comprise the tail boom structure. The skin consists of one circumferential wrap from Boom Station (B.S.) 32 to B.S. 46, one ± 60 degrees from B.S. 32 to B.S. 102, and two helical 25-degree layers for the full length (27 degrees for the flightworthy tail boom). The aft end of the tail boom is flat on the upper surface where the tail rotor gearbox attaches. A 2-inch-diameter cutout, reinforced with graphite doublers, is located at B.S. 84.57 to accommodate the horizontal stabilizer spar tube. An E-glass stiffening ring located at the forward end of the tail boom provides for attachment of the tail boom to the cabin section. E-glass plates and fittings for the tail rotor gearbox and bellcrank, and supports for the offset vertical fin, are located at the aft end.

FINITE ELEMENT MODEL

The Engineering Analysis Language (EAL) finite element computer program was used to formulate the mathematical model of the OH-58A composite tail boom. The tail boom skins were modeled with two-dimensional quadrilateral membrane and quadrilateral bending elements. Plate elements were used to model the forward attachment bulkhead, the horizontal stabilizer supports, and the vertical fin supports. Beam elements were used to model the integrally wound bulkhead rings. The tail boom model consisted of approximately 400 nodes, 500 elements, and 2300 degrees of freedom. A schematic of the finite element model is shown in Figure 2. Composite material properties which account for the different fiber orientations and layer stacking sequences along the tail boom were calculated using a lamina preprocessor computer program. Sensitivity studies of fiber orientation and fiber volume effects on stiffness and dynamic characteristics guided the modeling effort. In modeling the tail boom structure, the inertia effects of instrumentation and bungee cord attachment hardware were included in the mass distribution. The finite element model was developed and analyzed by personnel from the Aerostructures Directorate. Only highlights of the modeling effort are presented herein. Reference 2 describes, in detail, the finite element model development and analyses.

Material testing was also performed by Aerostructures Directorate personnel to validate the fiber orientation and fiber volume parameters input to the finite element analysis. Fiber wrap angle variations were small and introduced negligible changes to the material properties. However, fiber volume varied from 45 to 50 percent and changed tail boom natural frequencies by as much as 6 percent. The analysis results reported herein are based on 45 percent fiber volume.

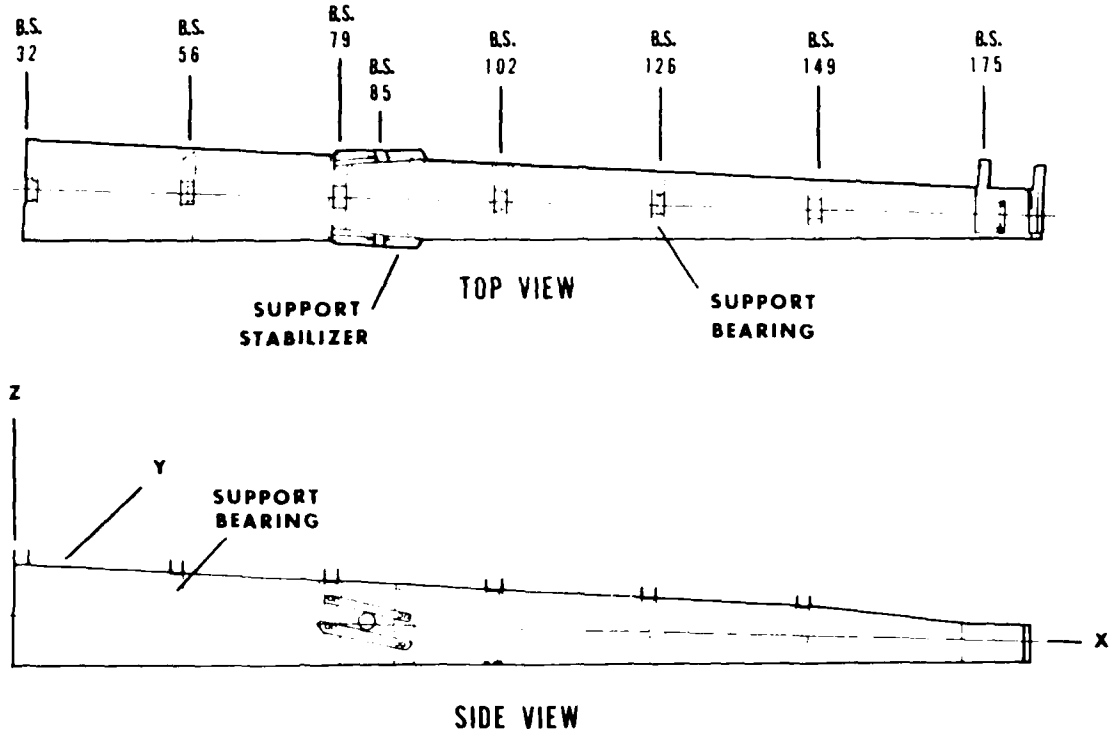

Figure 1. OH-58A composite tail boom.

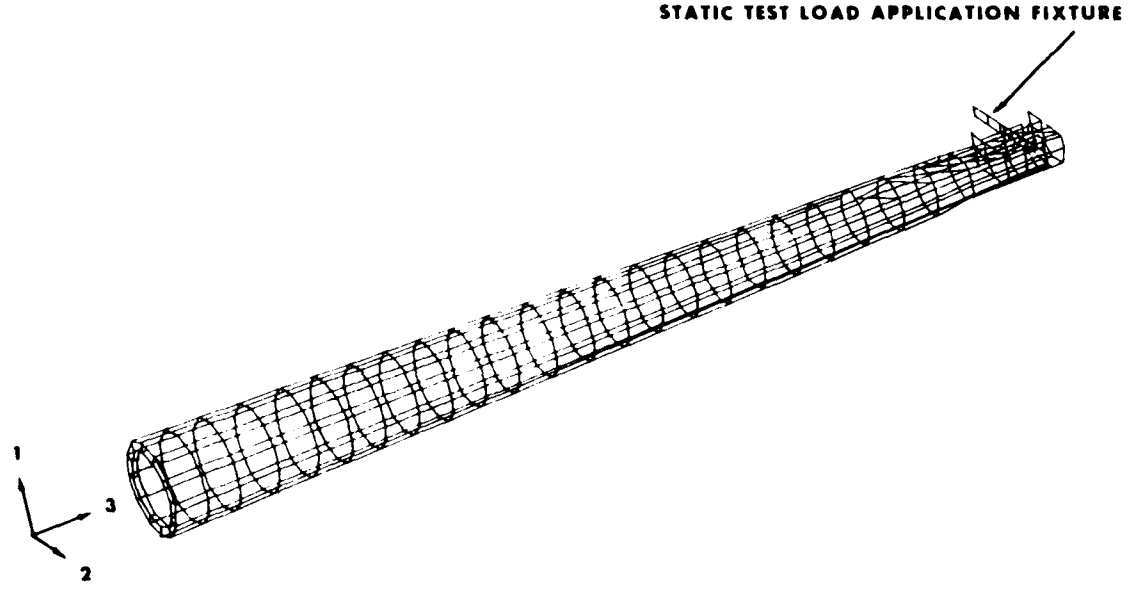

Figure 2. OH-58A composite tail boom finite element model.

STATIC TESTING

Independent static load/deflection tests were conducted on the tail boom in the vertical, lateral, and torsional directions. Results were compared with finite element calculations to substantiate the stiffness representation of the tail boom finite element model. Test setup, equipment and instrumentation requirements, data analysis, and results are discussed.

TEST CONFIGURATION AND PROCEDURES

The tail boom was inverted and cantilevered from a rigid backstop in the AATD Structures Laboratory Vibration Test Facility. A load application attachment was bolted to the aft end of the tail boom (B.S. 179) using the mounting structure for the tail rotor gearbox as shown in Figure 3. The subject attachment was designed to accommodate vertical, lateral, and torsional loads.

Vertical and lateral loads were applied independently in 20-pound increments from zero to 300 pounds. The torsional loading was applied in 600 in-lb increments to a maximum value of 6000 in-lb. Loading values selected were considered to be reasonable levels for verification of the stiffness representation of the finite element model. The tests were repeated three times in each direction to confirm repeatability of results.

For each load setting, the displacement transducer outputs were processed and stored on digital magnetic tape. This procedure was repeated for all loading conditions, which included loading in one direction, releasing the load, loading in the opposite direction, and again releasing the load.

INSTRUMENTATION AND EQUIPMENT

For the vertical and lateral load/displacement tests, displacement transducers were placed at B.S. 88, 110, and 138. A 1000-pound capacity hydraulic actuator, with self-contained displacement monitoring capability and an attached load cell, was used to apply the required vertical and lateral loads at B.S. 179. Two 1000-pound hydraulic actuators were used to apply torsion at B.S. 179. A pointer was used to monitor any adverse displacement of the centroid of the tail boom's cross section at B.S. 183 as the couple was applied. Additionally, two displacement transducers were mounted at B.S. 32 on the upper and lower surfaces of the tail boom for the vertical test (see Figure 4) and on the right and left sides for the lateral test to monitor possible movement between the backstop plate and the tail boom. For the torsion test, the displacement transducers were placed at 45 and 225 degrees with respect to the tail boom vertical axis to monitor rotational movement.

DATA ANALYSIS AND TEST RESULTS

The data analysis was performed for selected load increments. Displacement readings at B.S. 32 were averaged separately for vertical and lateral loadings at each load increment, and the vertical and lateral displacements at each station of interest caused by end fixity discrepancies were calculated and removed from the respective displacement readings for each load increment to obtain only elastic displacements. Tables 1 and 2 and Figures 5 and 6 show representative elastic displacements obtained by applying increasing loads. Differences between static elastic displacement measurements and finite element calculated displacements ranged from 6 to 12 percent. The data obtained during load application and release were almost identical, indicating negligible hysteresis

effects on the material permanent set. Figure 7 identifies lateral node points of the EAL finite element model that correspond to the instrumented tail boom stations. Note that the load application fixture was included in the finite element model.

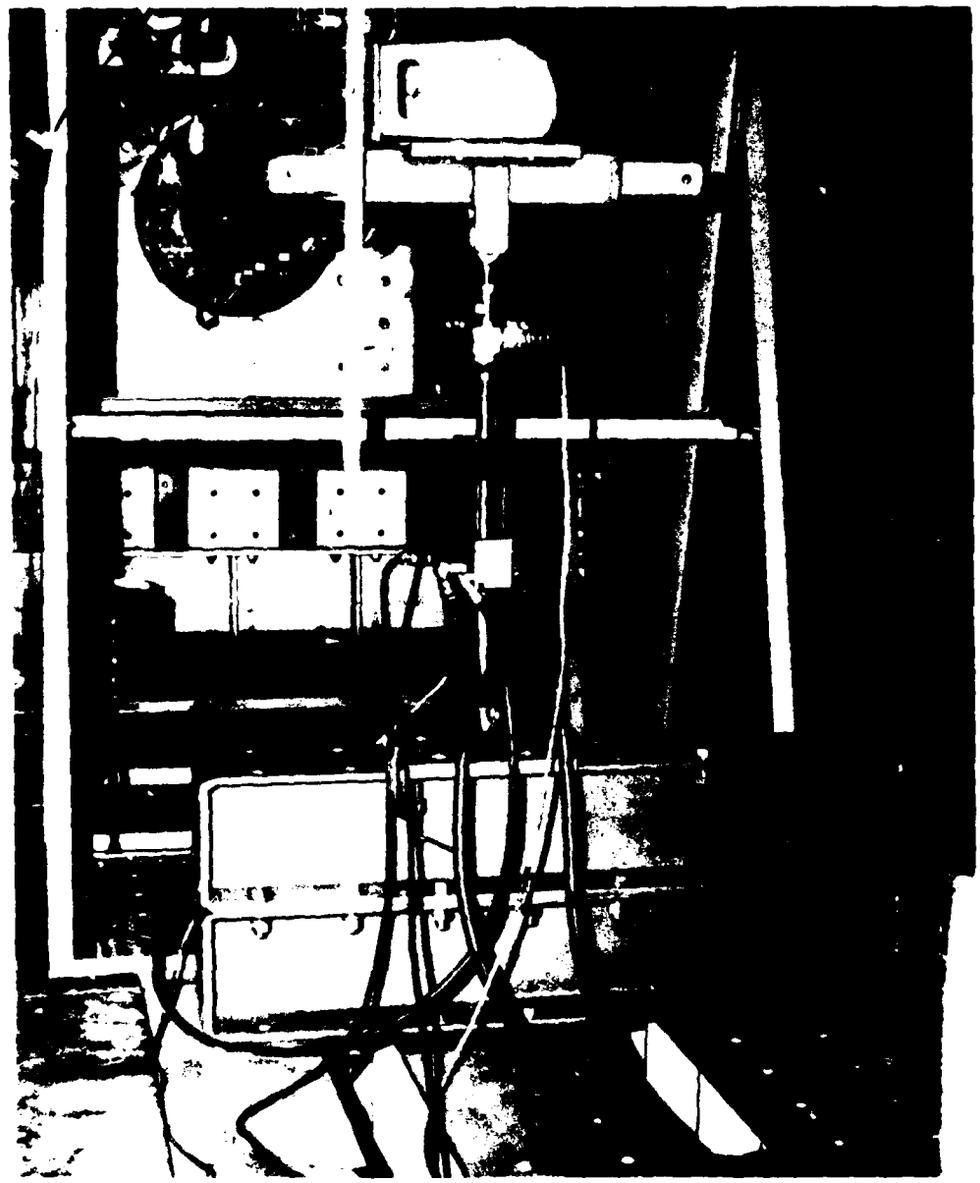

Figure 3. Static test setup, vertical load/deflection tests.

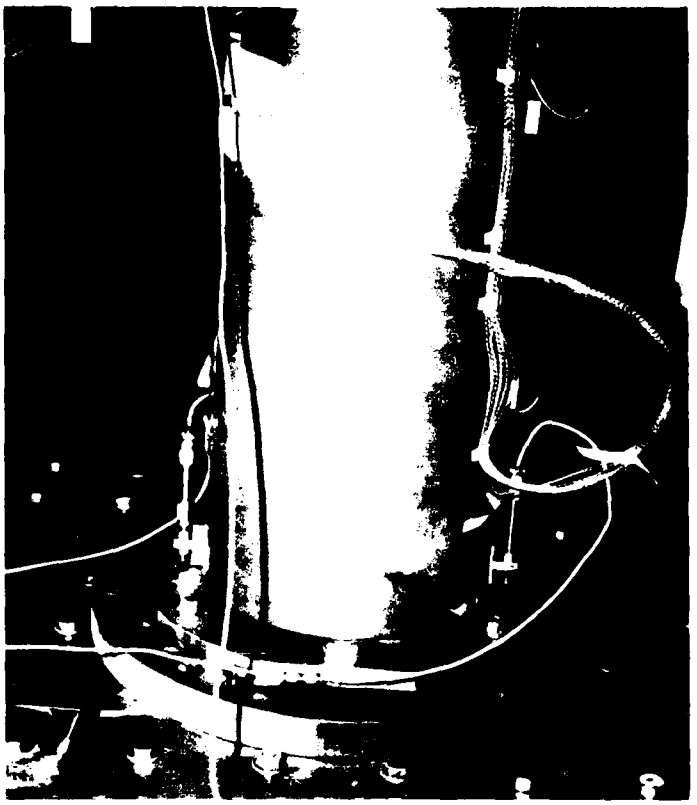

Figure 4. Instumentation at tail boom attachment (B.S. 32).

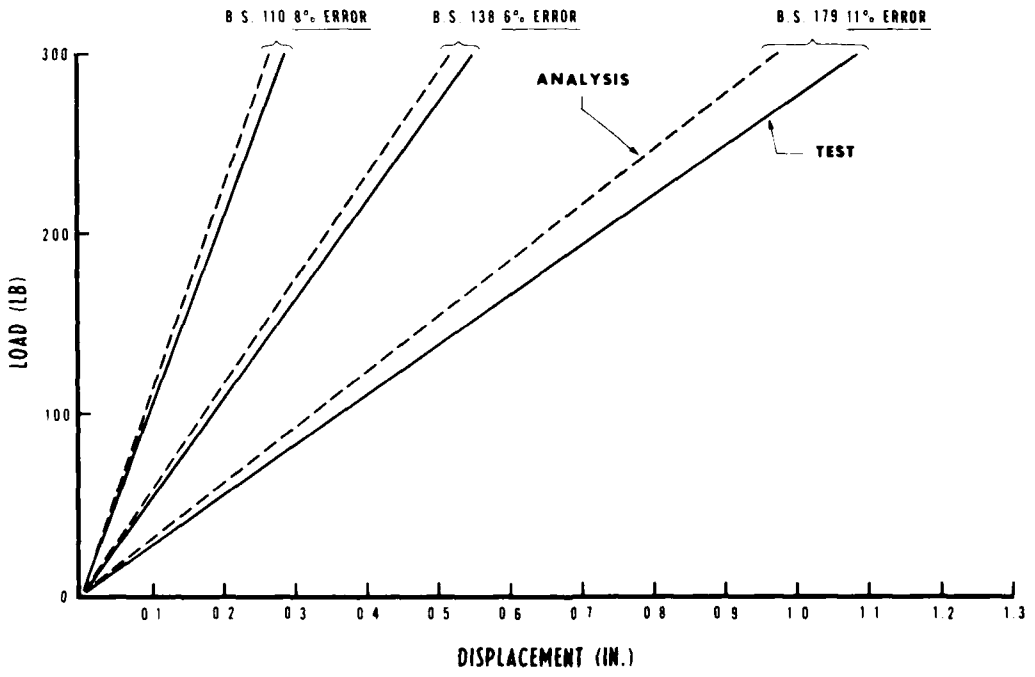

Figure 5. Analytical and test result comparisons, vertical load/deflection tests.

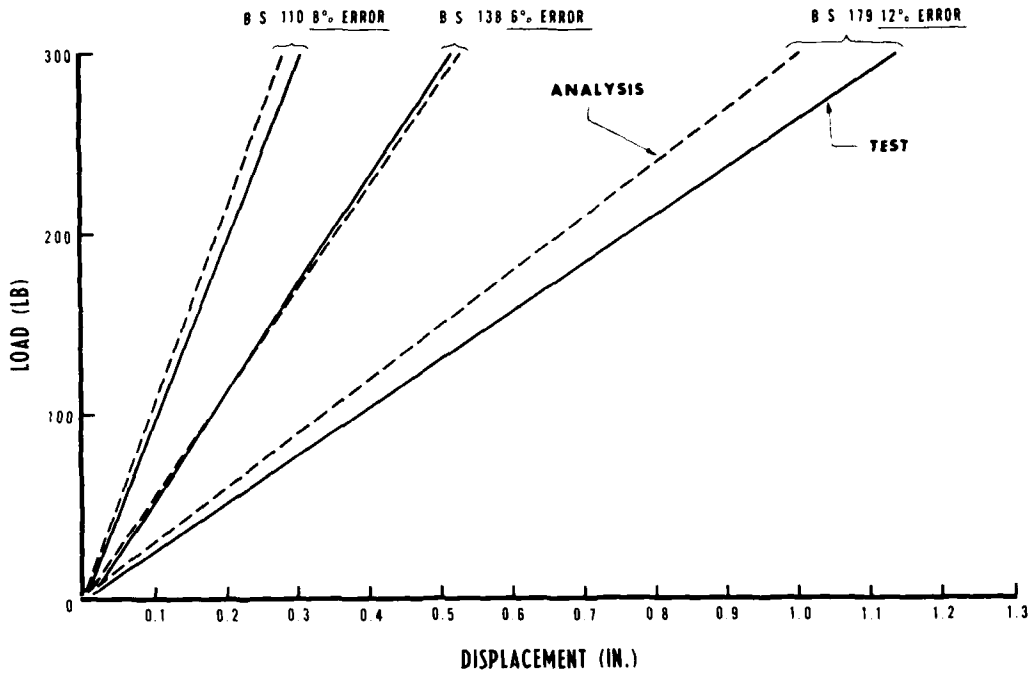

Figure 6. Analytical and test result comparisons, lateral load/deflection tests.

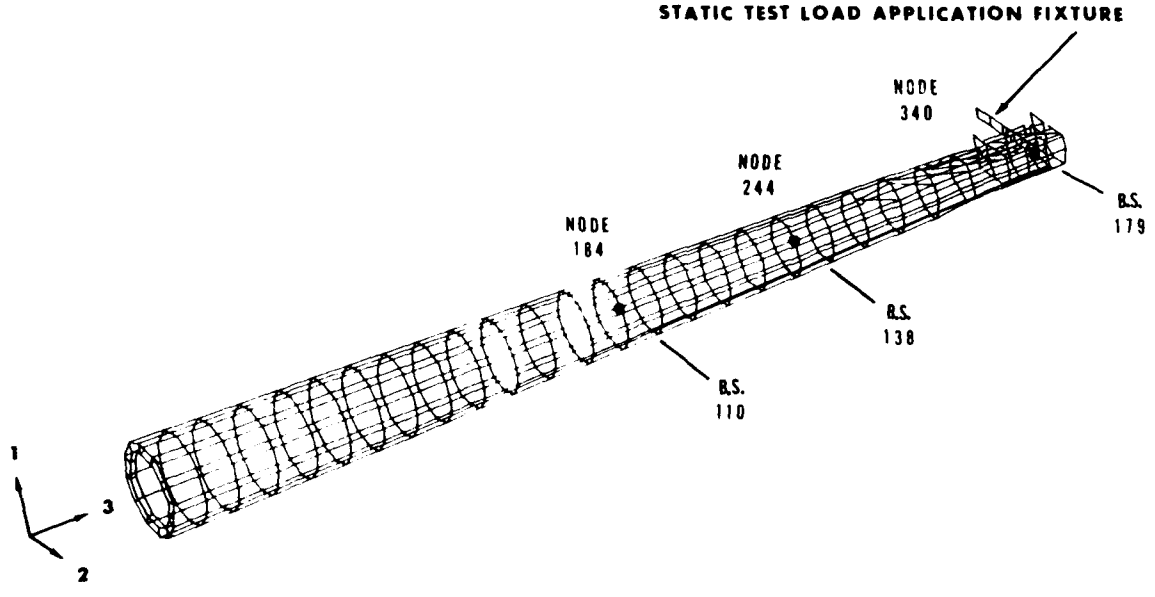

Figure 7. Model node identification and transducer locations for static tests.

TABLE 1. VERTICAL STATIC DEFLECTION COMPARISONS

Load (lb)	Displacement (in)					
	EAL Node 181	Test B.S. 110	EAL Node 241	Test B.S. 138	EAL Node 337	Test B.S. 179
40	-0.0375	-0.028	-0.0693	-0.0659	-0.1303	-0.1540
80	-0.0715	-0.070	-0.1386	-0.1404	-0.2605	-0.2861
140	-0.1251	-0.129	-0.2426	-0.2488	-0.4559	-0.4977
200	-0.1787	-0.186	-0.3466	-0.3573	-0.6513	-0.7376
260	-0.2323	-0.253	-0.4505	-0.4637	-0.8467	-0.9201
300	-0.2681	-0.288	-0.5199	-0.5497	-0.9769	-1.0896

TABLE 2. LATERAL STATIC DEFLECTION COMPARISONS

Load (lb)	Displacement (in)					
	EAL Node 184	Test B.S. 110	EAL Node 244	Test B.S. 138	EAL Node 340	Test B.S. 179
40	-0.0375	-0.0424	-0.0707	-0.0766	-0.1336	-0.1552
80	-0.0751	-0.0847	-0.1415	-0.1530	-0.2673	-0.3147
140	-0.1314	-0.1540	-0.2476	-0.2091	-0.4677	-0.5517
200	-0.1877	-0.2045	-0.3537	-0.3590	-0.6682	-0.7709
260	-0.2440	-0.2623	-0.4598	-0.4449	-0.8686	-0.9881
300	-0.2816	-0.3028	-0.5305	-0.4985	-1.0022	-1.1336

DYNAMIC TESTING

Vibration tests were conducted to measure acceleration mobility versus frequency. Modal analyses were performed on these data to determine vertical and lateral natural frequencies, modal damping, and orthonormal modes. The test-derived modal parameters were compared with parameters obtained from the finite element model calculations.

TEST CONFIGURATION AND PROCEDURES

The composite tail boom was suspended at two points (B.S. 32 and B.S. 183) using low spring rate bungee cords to simulate free-free boundary conditions. A system rigid body natural frequency below 1 Hz was achieved, which minimizes dynamic coupling of this mode with tail boom elastic responses. The test setup is shown in Figure 8. Initial shake tests were conducted with the horizontal stabilizer attached to the tail boom. The two piece stabilizer (see Figure 9) attaches to the tail boom with circular composite spar tubes/sleeves and is secured with support plates and bolts. This method of attachment was difficult to model, and testing showed extensive stabilizer/tail boom coupling in the test frequency range of interest. To avoid unnecessary complexity from both modeling and testing viewpoints, the horizontal stabilizer was removed. All dynamic test and analysis comparisons were performed for the tail boom only.

The vibration tests were conducted using a single-point swept sine excitation. The swept sine technique was achieved by applying a pure sine wave signal to an electromagnetic shaker and slowly varying the frequency of the sine wave over the frequency range of interest. These tests were performed with the shaker attached first at the forward (B.S. 32) and then at the aft (B.S. 183) end of the tail boom in both the vertical and lateral directions. Wideband (5 to 500 Hz) preliminary tests were conducted to obtain estimates of the natural frequencies. Narrowband testing was used in the vicinity of the identified modes to provide measurement accuracy and high frequency resolution required by modal analysis techniques. Prior to taking final data, the test specimen was vibrated at a low force level for several minutes. This "warm-up" time was necessary because of observed transfer function differences.

INSTRUMENTATION AND EQUIPMENT

As shown in Figure 10, the composite tail boom was instrumented with eleven piezoresistive accelerometers, seven vertically and four laterally. The accelerometers were mounted to aluminum blocks which conformed with the taper of the tail boom to assure that response vectors coincided with the relevant vertical and lateral reference axes. Accelerometers were placed diametrically opposite from the shaker attachments to check for driving-point local modes. In addition to the tail boom accelerometers, an impedance head was attached between the shaker and specimen. The impedance head, which incorporates a piezoelectric accelerometer and force gage, is capable of measuring driving-point frequency response.

An electromagnetic shaker, in conjunction with a sweep oscillator and servocontroller (to maintain constant load), was used to excite the structure. The transducer outputs were input to a digital signal analyzer where transfer functions were measured and stored.

TEST RESULTS

Preliminary vibration tests were conducted to obtain natural frequency estimates to check force versus mobility linearity, and to confirm reciprocity. Figures 11 through 16 show acceleration mobilities for wideband (5 to 500 Hz) testing. These figures indicate that the most significant modal activity occurs between 400 and 500 Hz, and the frequency range from 5 to 250 Hz contained the first two or three vertical and lateral modes. As expected, this frequency range is much greater than the frequency range of interest for typical helicopter airframe structures due to the boundary conditions used in the test. Figures 11 and 14 clearly define the first vertical and first lateral modes of the tail boom. Figures 12 and 15 present examples of driving-point local mode effects which make higher mode identification difficult. The local mode phenomenon is not as significant for transfer mobilities (see Reference 3). Figures 13 and 16 are transfer mobilities for vertical and lateral excitations. The second vertical and second lateral modes are identified from these responses. The spike in Figure 13(a) at about 300 Hz is a "center frequency glitch" caused by the digital signal analyzer. Because of the high frequency characteristics of the tail boom, correlation was performed only for the first two vertical and lateral elastic modes of vibration.

The force level selected for the vibration tests was guided by force versus mobility linearity tests previously performed on an OH-58A metal tail boom. Figure 17 shows that transfer mobilities off resonance for the metal tail boom do not change significantly for loads greater than 2.5 pounds. Based on these results, a force versus mobility linearity check for the composite tail boom was conducted in this force range. The force level selected for the ground vibration tests was 3.13 pounds.

Reciprocity tests were conducted to confirm symmetry between force and response stations, as required by a linear structure. The tail boom was excited vertically at B.S. 32 and vertical response was measured at B.S. 183. The excitation and response stations were interchanged and the test was repeated. Figures 18 and 19 show the results of reciprocity testing in the vicinity of the first and second vertical modes. The natural frequencies obtained from shaking at B.S. 183 were about 2.0 Hz lower than the natural frequencies obtained from shaking at B.S. 32. These differences can be attributed to changes in shaker-to-tail boom compliances at the excitation stations.

MODAL ANALYSIS

Narrowband testing was conducted for the first and second vertical modes and the first and second lateral modes. Figures 20 through 22 show typical narrowband mobility plots. These narrowband data were used to identify tail boom natural frequencies, modal damping and orthonormal modes. Various techniques have been developed for estimating natural frequencies and modal damping. For this study, natural frequencies were determined from the peak of the imaginary mobility, and the modal damping was determined using the half-power method. Reference 3 discusses other techniques for determining these modal parameters. The orthonormal modes were determined using the matrix difference algorithm also presented in Reference 3. The computational scheme requires mobility data at discrete frequencies as well as natural frequency and modal damping at each mode of interest. The discrete frequency mobility inputs to the software are summarized in Tables 3 through 6. The natural frequency and modal damping inputs, also shown in Tables 3 through 6, were obtained by using the average of values from all transducers. Limited checks of the orthonormal modes calculated by using local values of natural frequency and modal damping showed differences between 2 and 5 percent with respect to orthonormal modes using average values for frequency and damping. Based on the results of this study, it appears that the matrix difference method is well suited for processing data from large numbers of transducers for modal analysis.

TEST AND ANALYSIS COMPARISONS

The finite element model was used to calculate natural frequencies and orthonormal modes for the composite tail boom assuming free-free boundary conditions. The modal analysis of the shake test data provided natural frequency and orthonormal mode measurements for correlation purposes. Natural frequency comparisons between test and analysis for the first and second vertical and lateral modes of vibration are shown in Figure 23. These natural frequencies are much higher than the frequency range of interest for typical helicopter airframe structures. Nevertheless, the composite tail boom was analyzed and tested without adding mass or changing boundary conditions to lower the natural frequencies.

Differences in natural frequencies were between 1 and 5 percent for the first vertical and lateral modes and between 1 and 3 percent for the second vertical and lateral modes. These differences in natural frequency placement between test and analysis results are within acceptable accuracy limits of finite element model correlation studies. Interpretation of test and analysis data to identify the first vertical and lateral modes and the second lateral mode was straightforward. However, second vertical mode definition was more difficult because two modes, one at 221 Hz and one at 227 Hz, were identified from analysis. Examination of the analytical responses around the circumference of the tail boom revealed significant variations near the aft end (B.S. 149 and outward), suggesting that the model needs to be improved in that area. The analytical 227 Hz mode was selected as the second vertical mode because the tail boom mode shape was consistent with a free-free second mode shape. Comparisons of the first two vertical and lateral orthonormal modes are presented in Tables 7 and 8. The finite element model node points used in the comparisons correspond to accelerometer locations that are shown in Figure 10. Tables 7 and 8 demonstrate a consistency between the shake test results and the finite element calculations for first vertical and first lateral orthonormal modes. However, interpretation of test and analyses results for the second vertical and second lateral modes is complicated by two factors: the high frequency range imposed by the test configuration, and the modeling deficiencies at the aft end of the tail boom. Nevertheless, the results do show correlation of the second mode shapes.

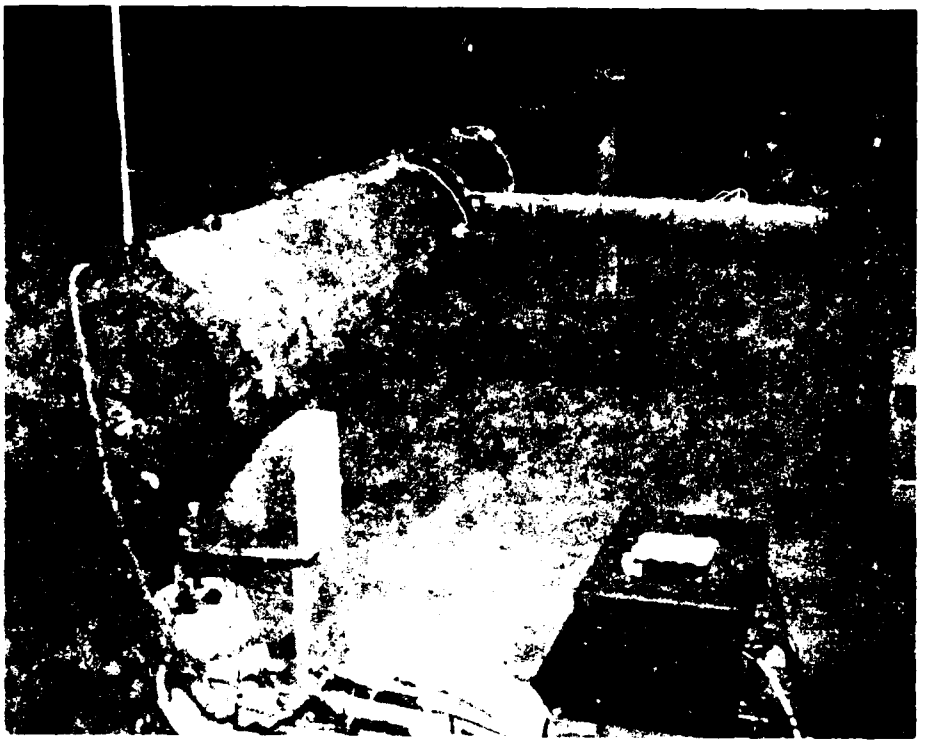

Figure 8. Dynamic test setup, vertical excitation.

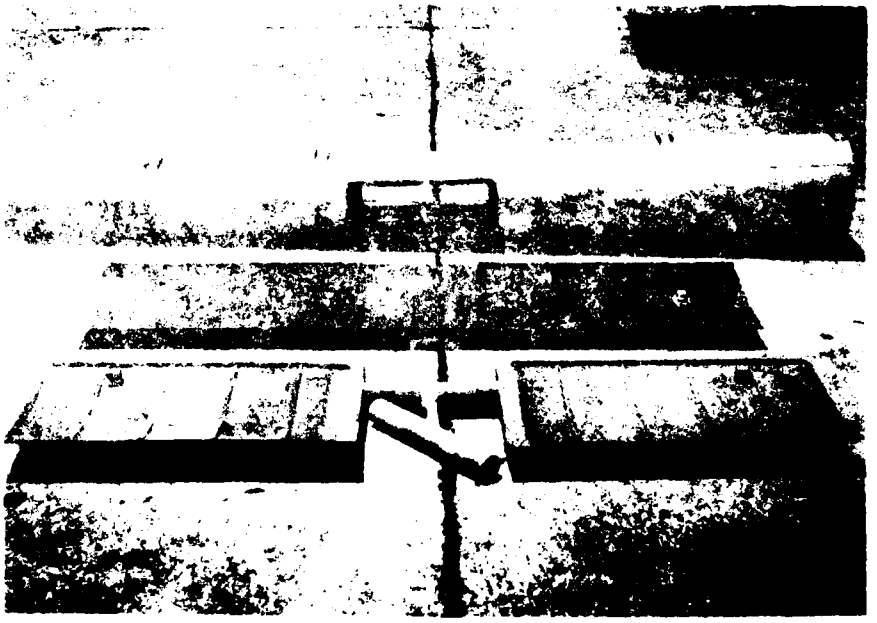

Figure 9. OH-58A composite horizontal stabilizer.

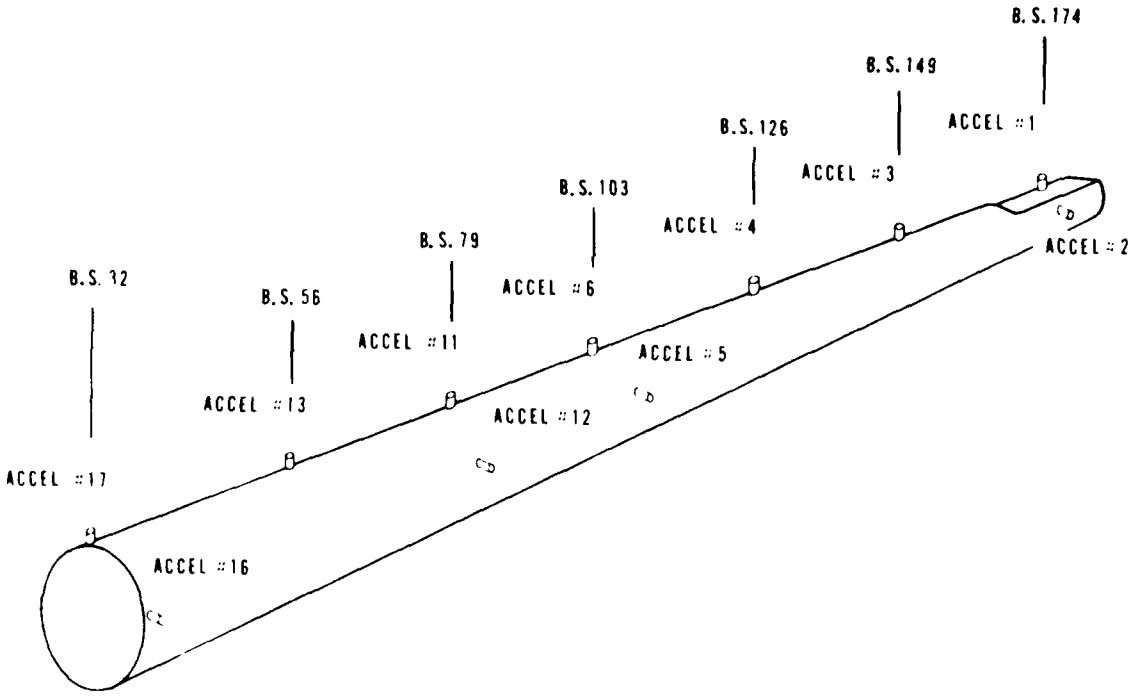

Figure 10. Tail boom accelerometer locations.

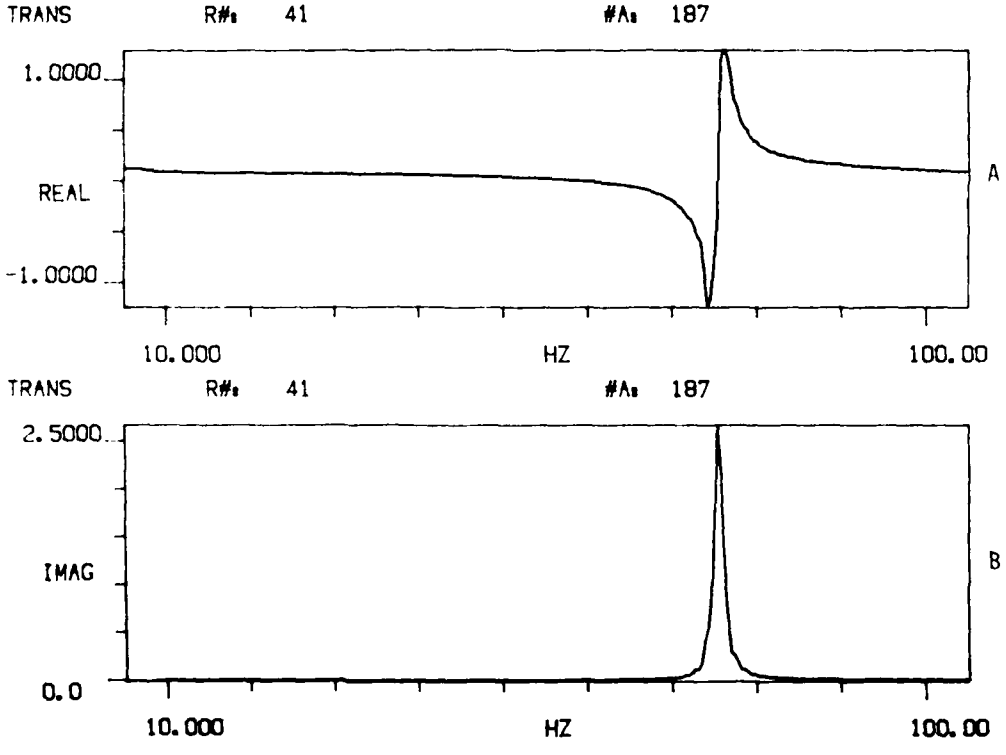

Figure 11. Driving-point response, vertical excitation at B.S. 32 (5 to 100 Hz).

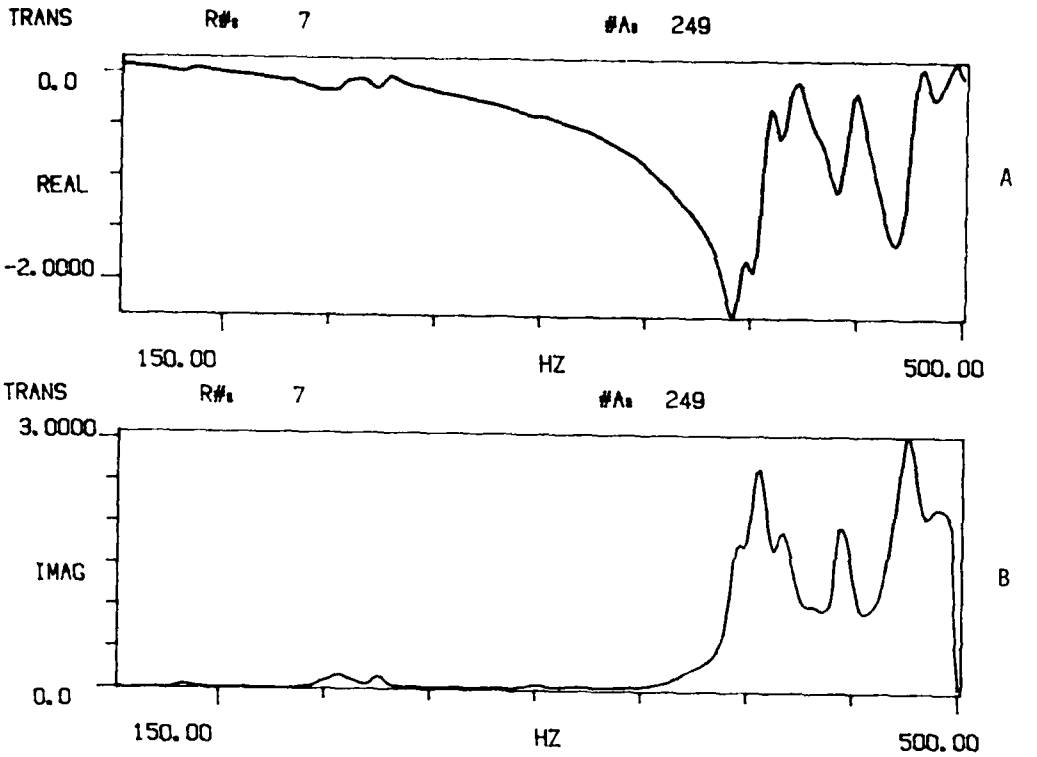

Figure 12. Driving-point response, vertical excitation at B.S. 32 (100 to 500 Hz).

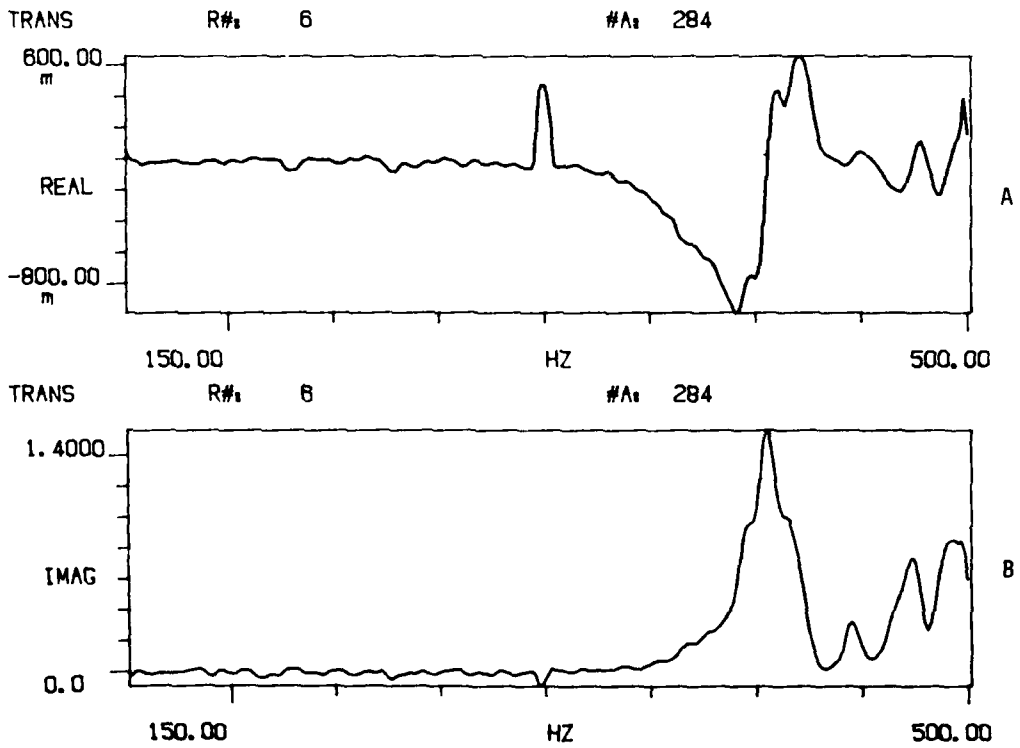

Figure 13. Transfer response, accelerometer no. 17, vertical excitation at B.S. 32 (100 to 500 Hz).

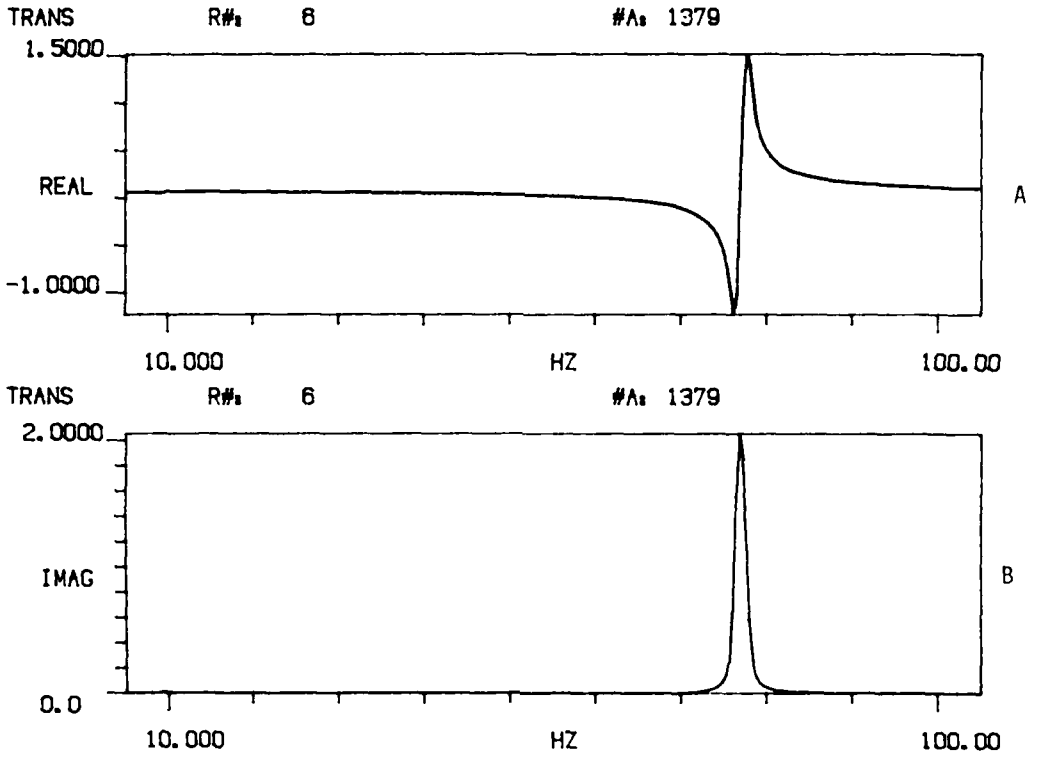

Figure 14. Driving-point response, lateral excitation at B.S. 32 (5 to 100 Hz).

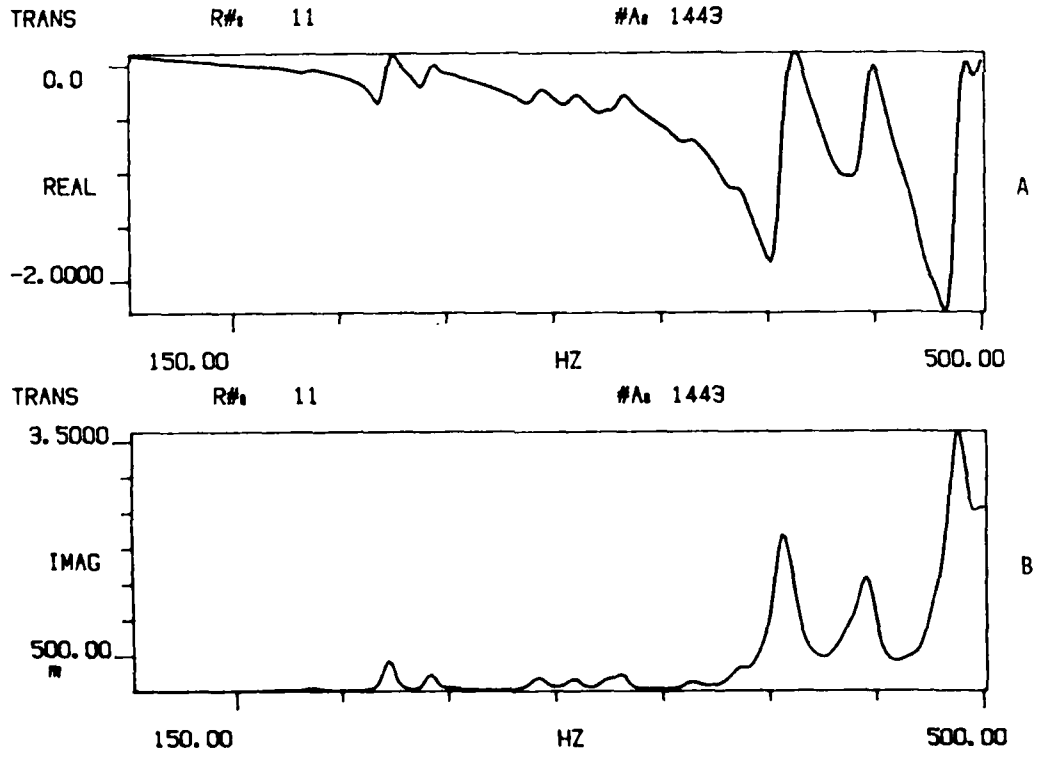

Figure 15. Driving-point response, lateral excitation at B.S. 32 (100 to 500 Hz).

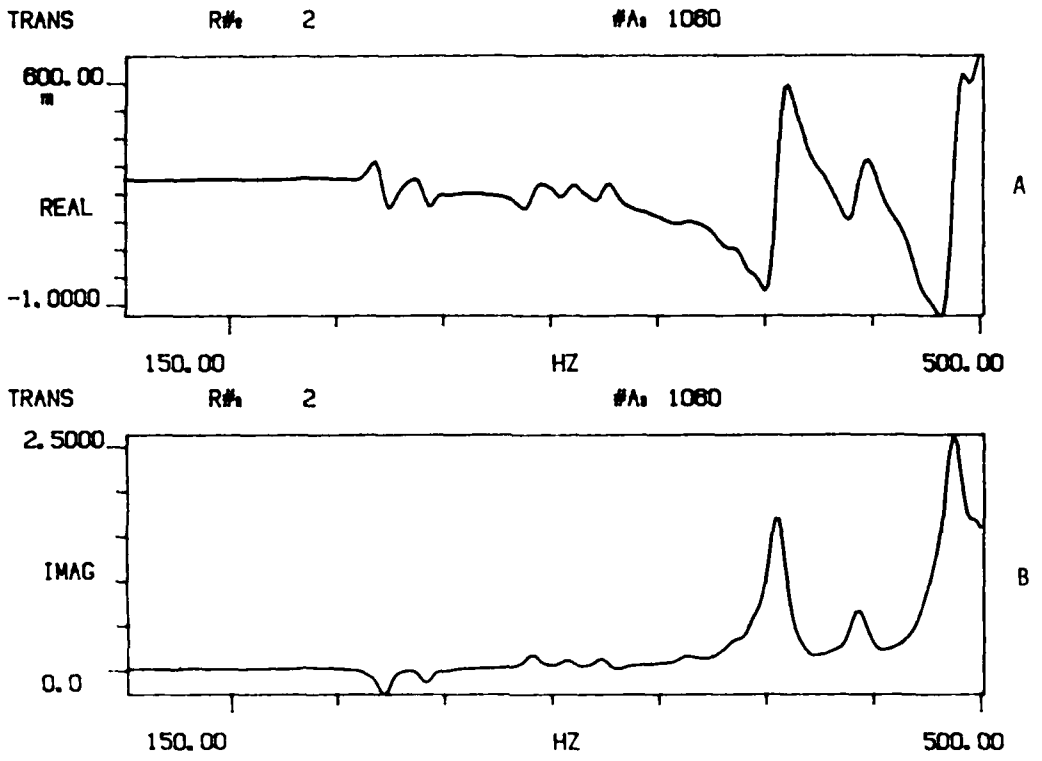

Figure 16. Transfer response, accelerometer no. 16, lateral excitation at B.S. 32 (100 to 500 Hz).

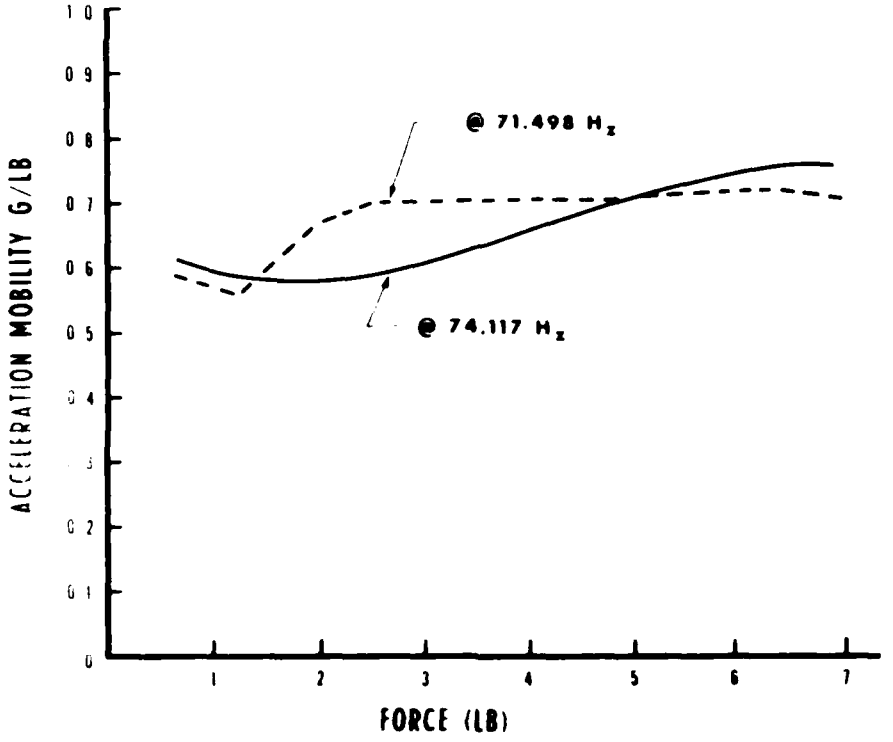

Figure 17. Acceleration mobility versus excitation force.

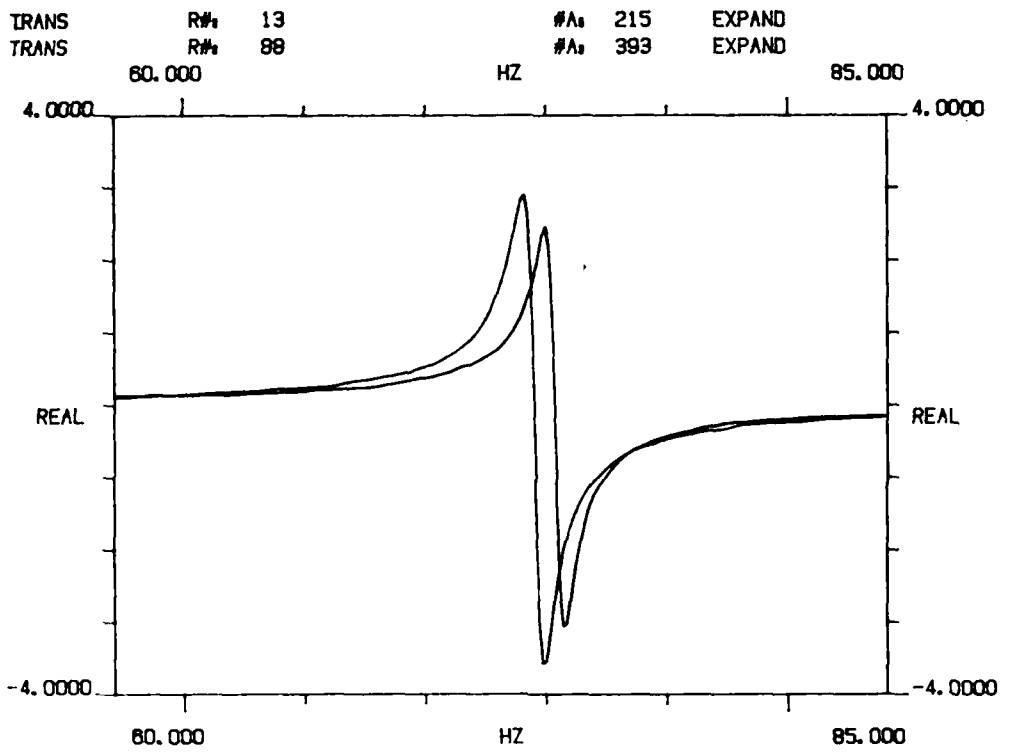

Figure 18. First vertical mode reciprocity testing, vertical excitation at B.S. 32 and B.S. 183.

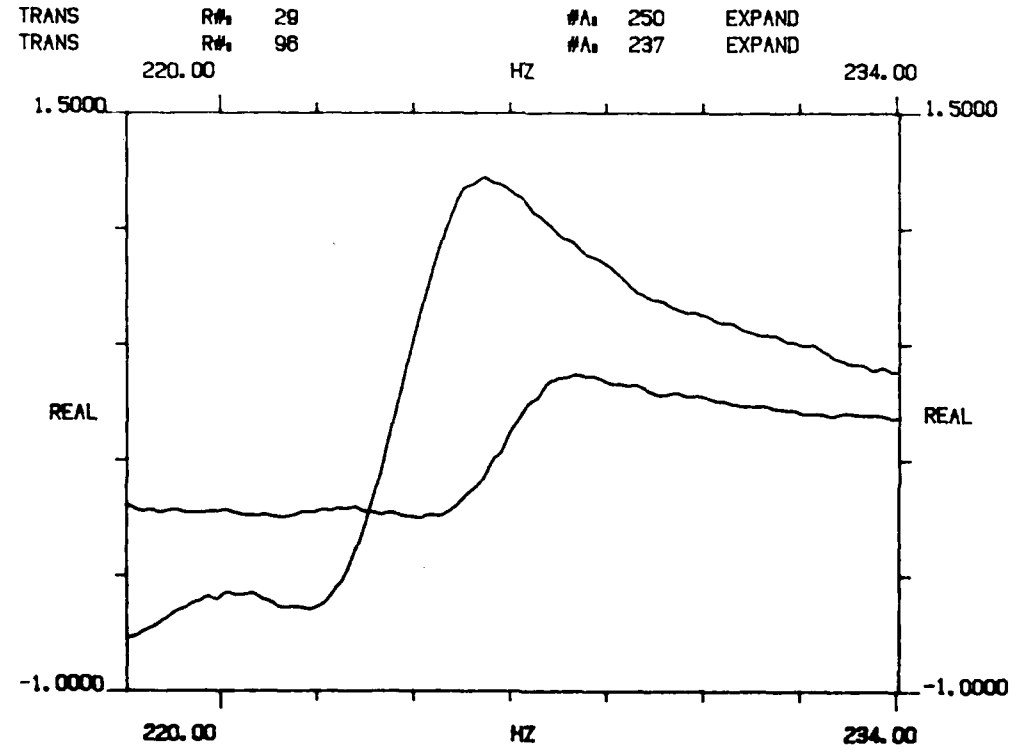

Figure 19. Second vertical mode reciprocity testing, vertical excitation at B.S. 32 and B.S. 183.

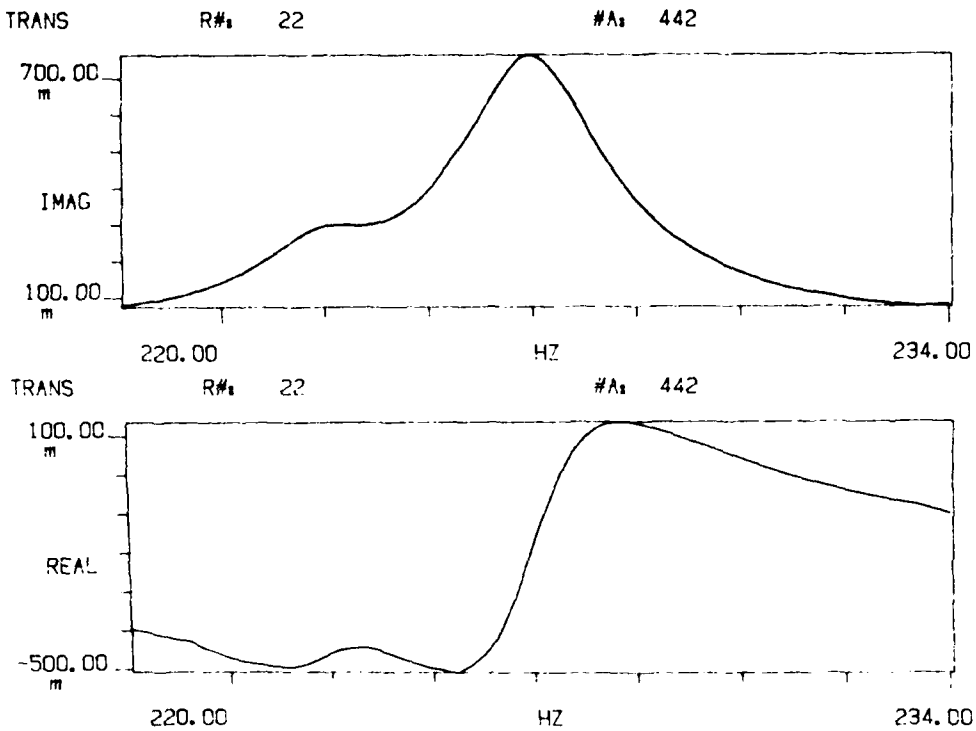

Figure 20. Second vertical mode narrowband driving-point response.

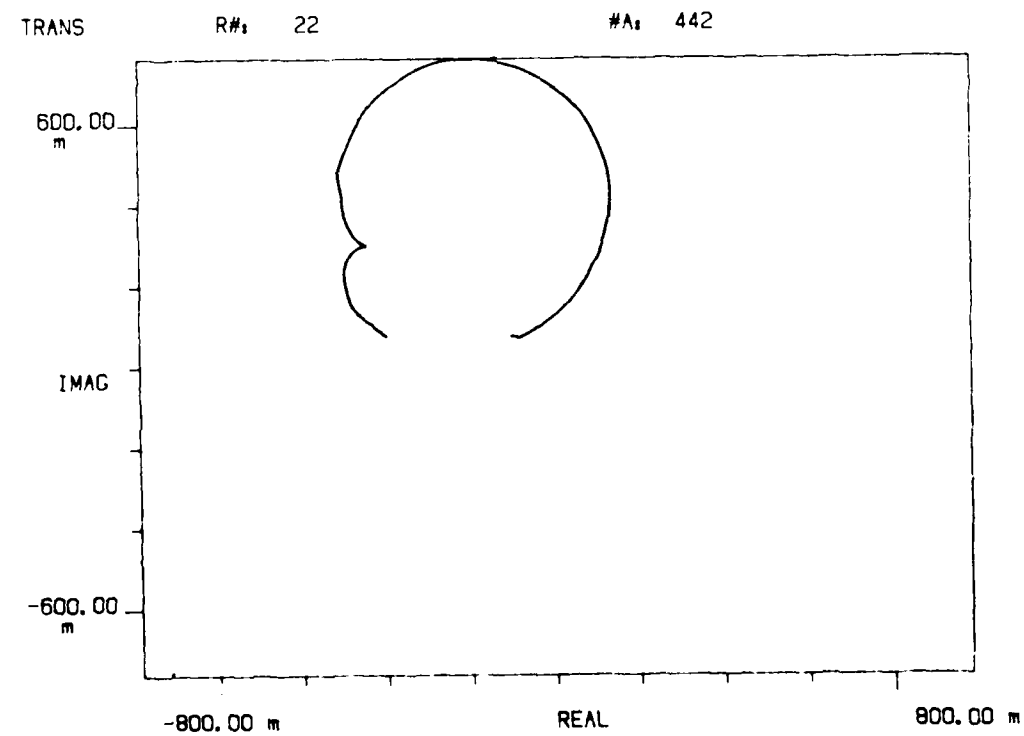

Figure 21. Second vertical mode narrowband driving-point response (Nyquist plot).

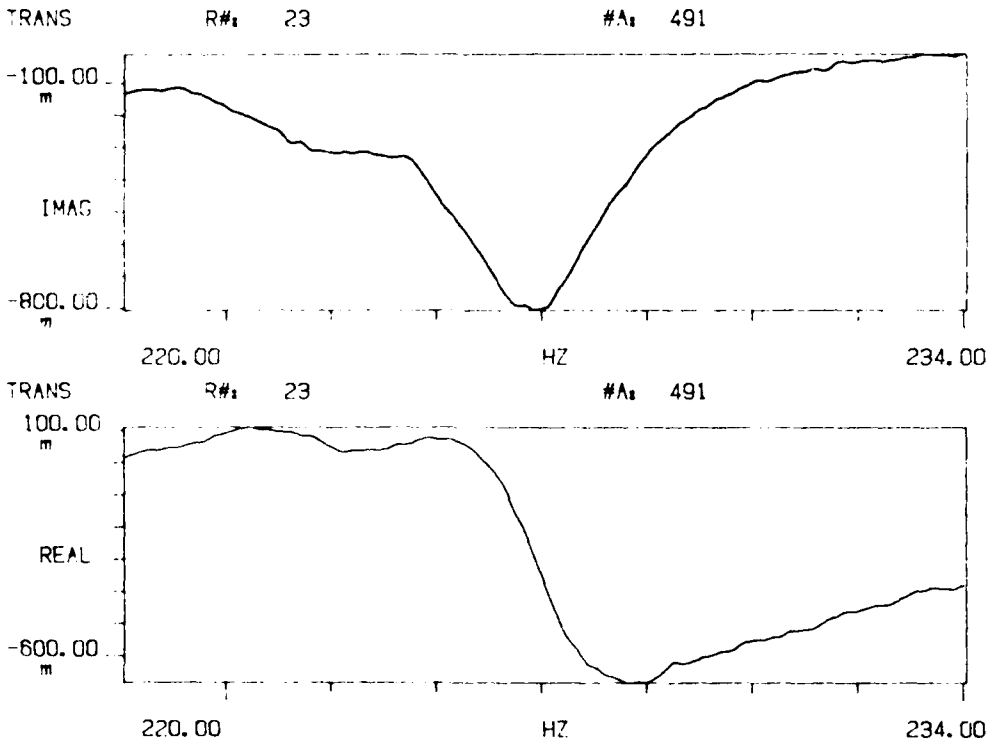

Figure 22. Second lateral mode narrowband transfer-point response.

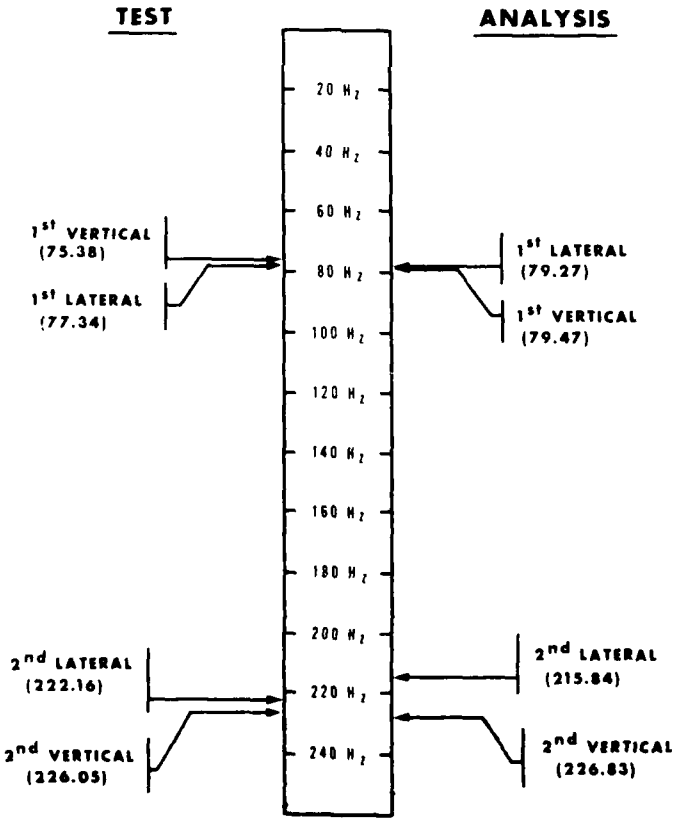

Figure 23. Test and analysis natural frequency comparisons.

TABLE 3. VERTICAL ACCELERATION MOBILITIES, EXCITATION AT B.S. 32

Mode 1
(Natural Frequency—75.38 Hz, Damping—0.011)

	Low Freq (75.00 Hz) Accel Mobilities		High Freq (75.75 Hz) Accel Mobilities	
Accels	Real (g)	Imag (g)	Real (g)	Imag (g)
Imped	-2.184	2.011	2.404	2.094
13	-0.032	0.099	0.221	0.131
11	1.392	-1.536	-1.644	-1.696
6	2.038	-2.326	-2.568	-2.538
4	1.927	-2.246	-2.481	-2.417
3	0.160	-0.200	-0.258	-0.234
1	-2.458	2.827	3.068	3.029

Mode 2
(Natural Frequency—226.05 Hz, Damping—0.016)

	Low Freq (224.22 Hz) Accel Mobilities		High Freq (227.50 Hz) Accel Mobilities	
Accels	Real (g)	Imag (g)	Real (g)	Imag (g)
Imped	-0.508	0.466	0.135	0.436
13	0.201	-0.328	-0.285	-0.345
11	0.278	-0.623	-0.694	-0.594
6	0.051	-0.228	-0.291	-0.113
4	-0.967	1.578	1.688	1.567
3	-0.746	1.102	1.046	0.118
1	0.240	-0.453	-0.373	-0.363

TABLE 4. VERTICAL ACCELERATION MOBILITIES, EXCITATION AT B.S. 183

Mode 1
(*Natural Frequency*–74.49 Hz, *Damping*–0.011)

	Low Freq (74.125 Hz) Accel Mobilities		High Freq (74.875 Hz) Accel Mobilities	
Accels	Real (g)	Imag (g)	Real (g)	Imag (g)
17	-2.8984	3.4599	3.5716	3.5810
13	-0.2112	0.2388	0.2221	0.2521
11	2.1572	-2.5911	-2.7112	-2.6670
6	3.3033	-4.0124	-4.2397	-4.0494
4	3.2169	-3.8724	-4.0380	-3.8933
3	0.5407	-0.5126	-0.4035	-0.5176
Imped	-5.8976	5.8963	6.7160	5.6680

Mode 2
(Natural Frequency–223.93 Hz, Damping–0.019)

	Low Freq (221.89 Hz) Accel Mobilities		High Freq (225.56 Hz) Accel Mobilities	
Accels	Real (g)	Imag (g)	Real (g)	Imag (g)
17	0.6465	-1.2845	-1.2212	-1.0461
13	-0.2978	0.7785	0.8341	0.6223
11	-0.7759	1.6497	1.6108	1.4003
6	-0.2909	0.5489	0.5217	0.5088
4	2.1329	-3.8023	-4.2670	-3.6830
3	1.4570	-2.9999	-2.8391	-2.4329
Imped	-2.1505	3.0487	2.8206	2.6440

TABLE 5. LATERAL ACCELERATION MOBILITIES, EXCITATION AT B.S. 32

Mode 1
(Natural Frequency—77.34 Hz, Damping—0.019)

	Low Freq (76.1720 Hz) Accel Mobilities		High Freq (77.7340 Hz) Accel Mobilities	
Accels	Real (g)	Imag (g)	Real (g)	Imag (g)
Imped	-1.233	0.659	1.516	1.218
12	0.780	-0.509	-0.945	-0.748
5	1.226	-0.823	-1.552	-1.124
2	1.420	0.955	1.763	1.320

Mode 2
(Natural Frequency—222.16 Hz, Damping—0.012)

	Low Freq (220.43 Hz) Accel Mobilities		High Freq (223.20 Hz) Accel Mobilities	
Accels	Real (g)	Imag (g)	Real (g)	Imag (g)
Imped	-0.471	0.405	0.237	0.364
12	0.363	-0.473	-0.557	-0.475
5	0.050	-0.071	-0.151	-0.125
2	0.217	-0.249	-0.214	-0.274

TABLE 6. LATERAL ACCELERATION MOBILITIES, EXCITATION AT B.S. 183

Mode 1
(Natural Frequency—75.39 Hz, Damping—0.02)

	Low Freq (75.39 Hz) Accel Mobilities		High Freq (76.95 Hz) Accel Mobilities	
Accels	Real (g)	Imag (g)	Real (g)	Imag (g)
16	-2.29300	1.61300	2.62500	1.40900
12	1.62840	-1.15900	-1.88100	-1.03810
5	2.64650	-1.89700	-3.01940	-1.63670
Imped	-4.53160	2.73520	5.05240	3.25730

Mode 2
(Natural Frequency—220.25 Hz, Damping—0.015)

	Low Freq (218.75 Hz) Accel Mobilities		High Freq (221.75 Hz) Accel Mobilities	
Accels	Real (g)	Imag (g)	Real (g)	Imag (g)
16	0.56990	-0.56390	-0.27620	-0.66120
12	-0.85630	0.90090	0.60120	1.00870
5	-0.27890	0.24770	0.05590	0.27230
Imped	-1.38240	1.41030	1.02690	1.49060

TABLE 7. VERTICAL ORTHONORMAL MODE COMPARISONS

Vertical Excitation at B.S. 32		Vertical Excitation at B.S. 183		EAL	
Mode 1					
Natural Frequency – 75.38 Hz Damping Coefficient – 0.011		Natural Frequency – 74.49 Hz Damping Coefficient – 0.011		Natural Frequency – 79.47 Hz	
Accel	Mode	Accel	Mode	Node	Mode
Imped	4.378	17	3.831	25	3.66
13	0.243	13	0.258	73	0.361
11	-2.901	11	-2.883	121	-2.28
6	-4.399	6	-4.466	169	-3.72
4	-4.209	4	-4.296	217	-3.28
3	-0.400	3	-0.559	265	-0.281
1	5.276	-	-	-	3.94
-	-	Imped	7.470	-	-
Mode 2					
Natural Frequency – 226.05 Hz Damping Coefficient – 0.016		Natural Frequency – 223.93 Hz Damping Coefficient – 0.019		Natural Frequency – 226.83 Hz	
Accel	Mode	Accel	Mode	Node	Mode
Imped	1.996	17	-2.288	25	1.26
13	-1.508	13	1.389	73	-0.84
11	-3.015	11	2.917	121	-1.48
6	-1.119	6	0.988	169	-0.12
4	8.231	4	-7.781	217	9.73
3	5.556	3	-5.267	265	0.515
1	-1.92	-	-	313	-10.9
-	-	Imped	6.063	-	-

TABLE 8. LATERAL ORTHONORMAL MODE COMPARISONS

Lateral Excitation at B.S. 32		Lateral Excitation at B.S. 183		EAL	
Mode 1					
Natural Frequency – 77.34 Hz Damping Coefficient – 0.019		Natural Frequency – 76.27 Hz Damping Coefficient – 0.020		Natural Frequency – 79.27 Hz	
Accel	Mode	Accel	Mode	Node	Mode
Imped	4.549	16	5.110	28	3.58
12	-2.824	12	-3.645	124	-2.21
5	-4.531	5	-5.888	172	-3.66
2	5.195	-	-	316	3.97
-	-	Imped	9.964	-	-
Mode 2					
Natural Frequency – 222.16 Hz Damping Coefficient – 0.012		Natural Frequency – 220.25 Hz Damping Coefficient – 0.015		Natural Frequency – 215.84 Hz	
Accel	Mode	Accel	Mode	Node	Mode
Imped	1.832	16	-0.825	28	2.68
12	-2.376	12	1.416	124	-3.27
5	0.538	5	0.325	172	-0.80
2	-1.114	-	-	316	-0.83
-	-	Imped	2.337	-	-

CONCLUDING REMARKS

This research effort was conducted to evaluate testing and modeling complexities of composite structures. An OH-58A composite tail boom was modeled using the EAL finite element program and was statically and dynamically tested to obtain data for correlation. From a testing viewpoint, no complexities were identified that can be directly attributed to composites. Concerns relative to end fixity for the static test and dynamic test, such as shaker attachment and local panel motion, were similar to those for metal structures. The solid graphite laminae exhibited low damping (1.1%), approximately equal to the damping measured from an OH-58A metal tail boom during limited testing.

From a modeling viewpoint, complexities such as laminae representation, fiber volume, and non-uniform laminae thickness around the circumference and along the length of the tail boom made the finite element representation difficult. These modeling concerns are described in Reference 2.

Correlation between the static and dynamic test results and the analysis data was quite satisfactory. Differences in the static results are well within acceptable limits used in the industry, and the placement of natural frequencies was quite good. The calculated orthonormal modes from the test and the analysis data agree well except for the aft portion of the tail boom for the second vertical and lateral modes. The static test results indicated that a possible modeling discrepancy existed at the aft end of the tail boom model; this came to focus during calculation of the orthonormal mode shapes.

The matrix difference method was utilized to calculate the orthonormal modes. It uses mobilities at frequencies straddling the natural frequency and an average value of damping for each mode. Based on the results obtained, this method appears to be well suited for calculating the modes of a linear structure from a large number of transducers.

REFERENCES

1. Taha, S., R. Doerr, and R. H. Messinger, *Environmental Effects and Durability Evaluation of Advanced Composite Fuselage Structure*, Hughes Helicopters, Inc., USAAVRADCOM TR 82-D-18, Applied Technology Laboratory, US Army Research and Technology Laboratories (AVRADCOM), January 1983, AD B070815L.

2. Bowman, Lynn, *Effect of Measured Material Properties on the Finite Element Analysis of an OH-58 Composite Tail Boom*, USAAVSCOM TR 85-B-5, NASA TM 86430, Aerostructures Directorate, US Army Aviation Research and Technology Activity (AVSCOM), to be published.

3. Giansante, N., A. Berman, W. G. Flannelly, and E. J. Nagy, *Structural System Identification Technology Verification*, Kaman Aerospace Corporation, USAAVRADCOM TR 81-D-28, Applied Technology Laboratory, US Army Research and Technology Laboratories (AVRADCOM), November 1981, AD A109181.

END

FILMED

12-85

DTIC